Improvement of O 2 plasma etching for diamond power MOSFET fabrication

Raid Gourad, Ralph Makhoul, Karine Isoird, Josiane Tasselli, Alain Cazarré, Aurélie Lecestre, Mathieu Arribat

Improvement of O_2 plasma etching for diamond power MOSFET fabrication

Raid GOURAD, Ralph MAKHOUL, Karine ISOIRD, Josiane TASSELLI, Alain CAZARRE,

Aurélie LECESTRE, Mathieu ARRIBAT

LAAS-CNRS, Université de Toulouse, CNRS, UPS, Toulouse, France

1-Introduction

Diamond is a promising semiconductor material for the fabrication of high power electronic devices, due to its remarkable properties such as very high critical electric field (Ec ~ 10 MV/cm), high carriers mobilities (2200 cm^2/V.s for electrons and 2050 cm^2/V.s for holes). Moreover, its wide bandgap (Eg ~ 5.5 eV) and high thermal conductivity (20 W/cm.K) can be well exploited for a wide field of high temperature, high power applications [1].

The fabrication of diamond-based power devices such as a TMBS diode (Trench MOS Barrier Schottky diode) or a vertical P-channel MOSFET with U-gate (U-pMOS) [2] requires the development of critical technological steps, in particular diamond etching. Indeed, the aim is to get an accurate control of etching for defining the mesa of the TMBS diode and the U-shaped gate of the MOS transistor. Developing an etching process with anisotropic sidewalls and a resulting surface morphology with a low roughness is required to achieve the best performances of these devices.

Plasma etching is a key technique for diamond etching due to its high chemical inertness and mechanical strength [3-5]. Several techniques can be used such ion beam etching which can efficiently smoothen and polish single crystal diamond plates [6-7], plasma ion etching employed for deep etching [8-10], laser etching used to produce various grooves and holes of few micrometers size [11] and gas cluster ion beam to obtain smooth CVD diamond films applicable to devices [12]. Reactive ion etching (RIE) can be adapted to supply anisotropic etching with a better dimensional control of the etched patterns [13] according to a combination of physical and chemical etching mechanisms that depend on the plasma parameters [14].

We present the experimental results of oxygen-based ICP-RIE (Inductively Coupled Plasma - Reactive Ion Etching) etching of diamond layers, focusing on the impact of different etching masks, namely metallic (aluminum) and dielectric (SiO2) ones. Additionally, we examine the effects of bias power and ICP plasma power. Our study aims to prevent over-etching at the bottom of sidewalls, achieve high etch rates with smooth surface roughness, and ensure good etch selectivity between the mask and diamond. Furthermore, we investigate how the doping of diamond layers (p-type or n-type) and their crystalline quality influence the etch rate and the resulting surface morphology.

2-Plasma etching of diamond

It is possible with the ICP-RIE technique to control independently the ICP (Inductive Coupled Plasma) power (P_{ICP}), which acts on chemical etching via the plasma density, and the bias power (P_{Bias}) which influences the physical attack of the substrate via ions energy. Concerning the plasma pressure, a high pressure reduces the ions energy, thus favorizing chemical etching.

The choice of the etch mask plays a crucial role. It's mandatory to have a hard mask which can support the ions attack in order to avoid subsequent re-depositions that can occur on the diamond surface. These redeposited particles can act locally as a hard mask material preventing etching and resulting in the appearance of defects at the etched surface and a slowdown of the etch rate.

Various hard masks were used for diamond etching, in particular metallic masks such as Al [15,16], Au [17], Ni [18], and dielectric masks such as SiO_2 [19] and Si_3N_4 [20]. These masks were selected according to their selectivity.

Our previous experiments involved diamond etching using Ar/O_2 plasma with an aluminum hard mask to achieve etch depths higher than 10 µm. In this process, oxygen acts as the reactive specie responsible for chemical etching, while argon neutral species provide a physical component. This method achieved a high etch rate of 8.3 µm/h and a selectivity of 28, but the diamond surface was degraded by micromasking and trenching [21]. To overcome these problems, the Bosch method was used with Ar/O_2 + O_2/CF_4 plasma, which improved the surface morphology but did not eliminate the trenching [22].

Another etching process using O_2 plasma, which is primarily a chemical process, resulted in a smooth surface without micro-masking and vertical sidewalls. However, the etch rate was limited to 1.3 µm/h [23].

Although these processes have shown interesting results, they do not fully meet the requirements of TMBS or MOSFET U-gate fabrication. Our goal is to achieve an etch depth of 4 to 6 µm without trenching with a highest possible etch rate while maintaining surface integrity. The previously mentioned processes do not achieve this goal. Ar/O_2 plasma, despite its high etch rate, leads to surface degradation due to micromasking and trenching. The Bosch process improves the surface morphology but does not completely solve the trenching problem. Finally, although the O_2 plasma etching process provides a surface without micromasking and with vertical sidewalls, the etch rate is too low to achieve the desired depths.

In order to minimise or eliminate trenching, it is preferable to favour the chemical component of the etching process. Therefore, we decided to continue with O_2 plasma etching using ICP-RIE due to the encouraging results in terms of surface morphology and anisotropic etch profile, and therefore we have investigated the influence of plasma parameters, in particular ICP and bias power, using two types of masks: aluminum and silicon dioxide (SiO_2).

3- O_2 plasma etching with an aluminum mask

Diamond etching was performed on the Sentech SI500-DRIE equipment. The test samples were single crystal CVD diamond substrates of (100) orientation and 3 x 3 mm^2 size from Element Six.
The first step concerns chemical cleaning by solvents and acids to remove contaminations that could impact etching and the resulting roughness.
Diamond substrates were then coated with photoresist and insolated by laser lithography to define the mask pattern. An aluminum mask of 700 nm thick is then deposited by thermal evaporation. Metal thin films, such aluminum, are used as hard mask materials for single crystal diamond etching due to their good adhesion on diamond [24] and their good etching selectivity [25]. Moreover, a metal mask remains the better option compared to photoresist due to of its insufficient lifetime in the plasma particularly with the oxygen gas.

3.1Evaluation of O_2 plasma etching with P_{ICP} = 500W and P_{bias} = 5W

The first etching conditions we have studied are: P_{ICP} = 500 W, P_{Bias} = 5 W, pressure = 5 mT, gas flow rate = 25 sccm, temperature = 18°C. Each etching step is limited to 30

min to avoid self-heating created by the plasma on the surface of the sample.
We have reported on Fig 1 the variation of the etch rate as a function of etch time. Trenches of 1 µm deep were achieved after 2 h according to measurements with the mechanical profilometer. After 1 h, the etch rate stabilizes around 8 nm/min indicating that a bias power of 5 W is not useful for

Figure 1: Evolution of the etch rate versus etch time for an O_2 plasma at P_{ICP}= 500 W and P_{Bias} = 5W with an aluminum mask

etching trenches of 4 µm to 6 µm deep because a too long etch time would be necessary.

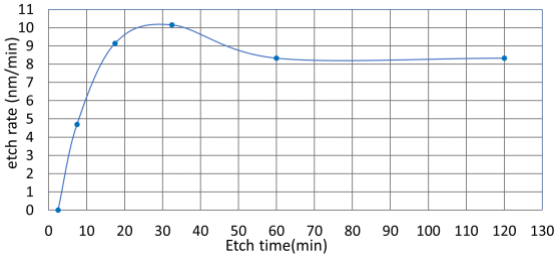

SEM views in Fig 2 show the surface state and the sidewall profile for etch times of 1 h (2 cycles of 15 min + one cycle of 30 min) and 2 h (4 cycles of 30 min). The etching profile is anisotropic, and a smooth diamond surface is obtained due to the absence of mask particles redeposition. The trenching is not observed after 2h of etching.
The ICP power was modified to 750 W to explore its impact on the etch rate which dropped from 8 nm/min to 2 nm/min. This is explained by the increase in the density of reactive oxygen species in the plasma, which results in the inability of ions to reach the diamond surface due to their low energy.

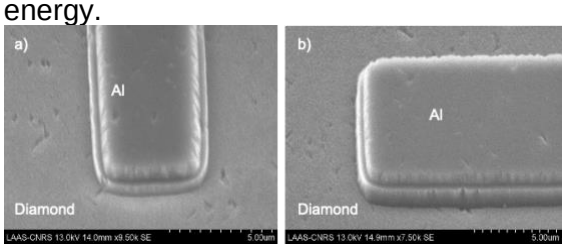

Figure 2: SEM views after different etch times with P_{ICP}= 500 W, P_{Bias} = 5 W a) after 1h of etching (3 cycles:15min/15min/30min); b) after 2h of etching (4 cycles of 30min)

3.2 Influence of the bias power P_{Bias}

In order to enhance the etch rate by increasing the effects of physical mechanisms, we chose to increase P_{Bias} from 5 W to 20 W, 35 W and 50 W for the ICP power fixed at 500 W.

The results obtained after 15 min etching are listed in Table 1. The diamond etch rate increased to 82 nm/min for a bias power of 50 W.

Table 1: Parameters of O_2 etching with an aluminum mask for different bias powers after 15 min etching

P_{Bias} (W)	**20**	**35**	**50**
Etch depth (µm)	0,63	0,95	1,22
Etch rate (nm/min)	42	65	82
Selectivity	33	21	11
Roughness before etching (nm)	3,3	1,8	1,5
Roughness after etching (nm)	7,9	3,5	6

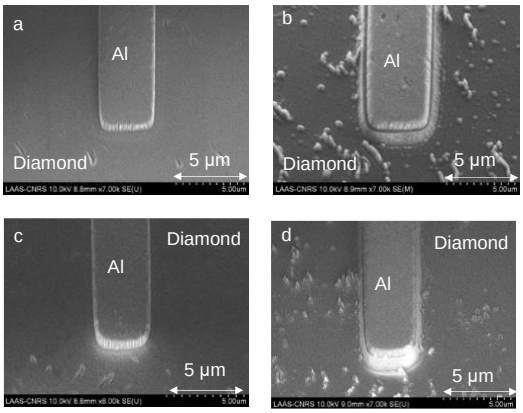

Figure 3: SEM images of the etching bottom and side before etching (a, b) and after O_2 etching with an aluminum mask for an etching time of 15 minutes at P_{ICP} = 500 W and for different bias powers: c) 35 W; d) 50 W

The surface roughness after etching increases considerably for a bias power of 50 W as shown on Fig 3. Furthermore, the trenching appears after 15 min (Fig 4). We can deduce that 35 W is the optimal bias power. The selectivity of the aluminum mask in this case is 21, etching rate is 65 nm/min and we don't note the presence of trenching. However, the surface roughness is increased by a factor of 2 from 1.8 nm before etching to 3 nm after. It can be explained by the defects produced by the

sputtered aluminum mask indicating that it is sensitive to the oxygen plasma.

4-Diamond etching with a SiO_2 mask

In order to reduce the micromasking mechanisms observed with an aluminum mask, we chosen to use a SiO_2 mask due to its low sensitivity to the oxygen plasma [14],[26]. Plasma parameters are the one optimized in the previous experiments: P_{ICP} = 500 W, P_{Bias} = 35 W pressure = 5mT, gas flow rate = 25 Sccm, temperature = 18 °C. A silicon oxide layer of 500 nm thick was first deposited by CCPECVD. After the patterning step by laser lithography, the SiO_2 mask was etched by ICP-RIE with a CHF_3 plasma under the following conditions: P_{ICP} = 500 W, P_{Bias} = 60 W and pressure = 5 mTorr.

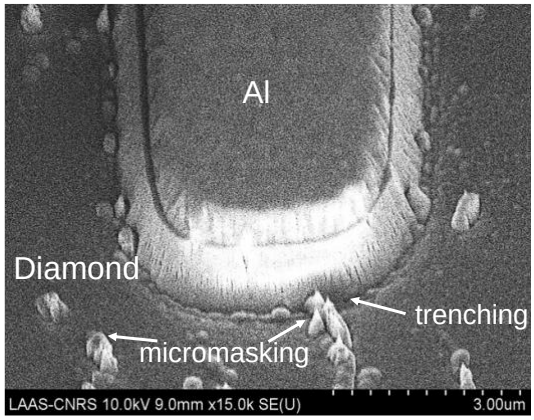

Figure 4: SEM image of O_2 etching with Aluminum mask at P_{ICP} = 500 W and P_{Bias} = 50 W for an etching time of 15 min.

4-1 Etching of unintentionally doped diamond layers

Figure 5 shows the AFM (Atomic Force Microscopy) observation of the diamond surface morphology after SiO_2 etching: a diamond roughness of 0.47 nm is measured instead of 0.39 nm before etching indicating that the surface is not damaged.

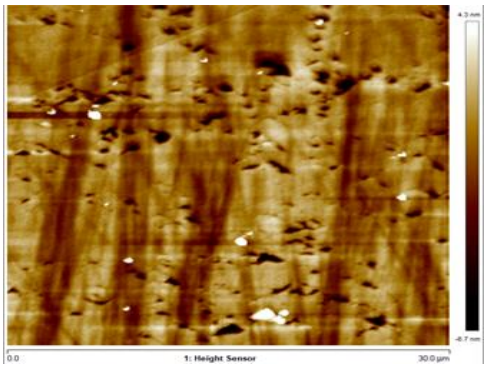

Figure 5: AFM image of the diamond surface after SiO_2 etching at P_{ICP} = 500 W, P_{Bias} = 60 W

In order to achieve a 6 µm deep diamond etching, and based on an etching rate of 4 µm/h for a bias power of 35 W, we carried out five O_2 cycles of 15 min each to achieve a full time of 75 min and the etch depth is measured after each cycle. Figure 6 indicates that the etching rate is stable during the etching cycles and its average value is approximately 75 nm/min.

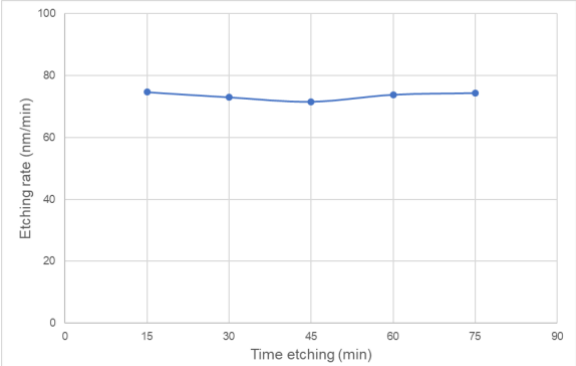

Figure 6 : Evolution of etching rate as a function of etch time for P_{ICP} = 500 W and P_{Bias} = 35 W with SiO_2 mask for intrinsic diamond layers

We have reported in Fig 7 a MEB view of the diamond surface after 15 min etching with the appearance of defects. This could be explained by the presence of oxide residues resulting from a too low etch time for the CHF_3 plasma performed to pattern the etching mask. These defects remain after the following cycles of O_2 plasma indicating that SiO_2 residues prevent diamond etching.

A step of O_2 plasma cleaning was added before CHF_3 plasma to verify that the micromasking was not produced by

photoresist residues due to an insufficient development during lithography: we observed the same defects after the O_2 plasma etching confirming that the observed residues are SiO_2 one.
In order to avoid the defects observed after diamond etching, an O_2 plasma cleaning is applied before SiO_2 etching and a short dip in buffered HF (BOE) was carried out after CHF_3 plasma to remove any oxide residues. Figure 8 shows the diamond surface state after an O_2 etching for 1h15 min (5 cycles of 15 min). No more defects due the SiO_2 mask sputtering are observed and the measured diamond depth is 6 µm.

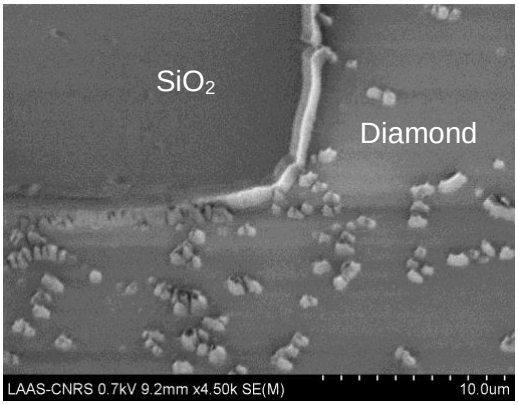

Figure 7: SEM image after 15 min diamond etching without BOE after SiO2 etching

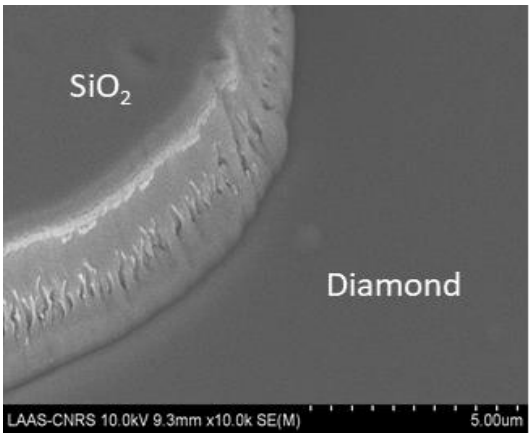

Figure 8: SEM image of diamond sidewall 1h15min O_2 etching with HF buffer cleaning after SiO_2 etching

After 2h45 min of etching (11 cycles), the etched depth is 12 µm both with no micromasking defects and no visible trenching in the SEM images at the bottom of the sidewall, confirming that a SiO_2 hard mask is a good candidate for diamond etching with an oxygen plasma.

As shown on the AFM measurements reported on Fig.9 we observed a slightly increase in the roughness from 0.43 nm for 15 min etching to 0.58 nm for 75 min.

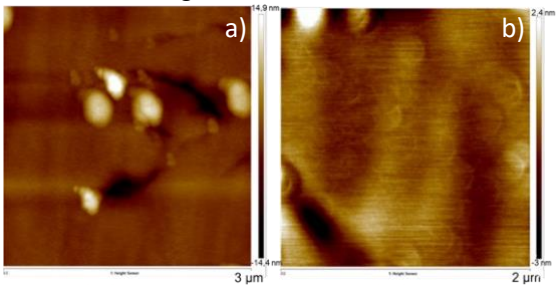

Figure 9: AFM images of diamond surface after O2 plasma for etching times of a) 15 min b) 75 min

The results indicate that the oxygen plasma with the optimum parameters i.e P_{ICP} of 500 W, P_{bias} of 35 W, a pressure of 5 mTorr and an O_2 gas flow of 25 sccm is a suitable way to overcome the trenching and the degradation of the surface quality. The SiO_2 hard mask has shown a strong resistance to O_2 plasma with a selectivity of 55.

4-2- Etching of P^- doped epitaxial diamond layers

We have investigated the influence of the etching process optimized in the previous section on a P^- doped epitaxial diamond layer of 6 µm thick, grown on 1b HPHT diamond substrate using microwave plasma chemical vapor deposition (MPCVD). SIMS measurements indicate a boron concentration of 10^{17} cm^{-3}.

Figure 10 illustrates the evolution of the etch rate (a) and the etch depth (b) over etching time. The etch rate of the P^- doped layer raises to 85 nm/min during the first ten minutes and decreases to achieve 73 nm/min after 1h30 min which is of the same order of magnitude as that for single-crystal CVD layers with the oxide mask (see Fig 6).

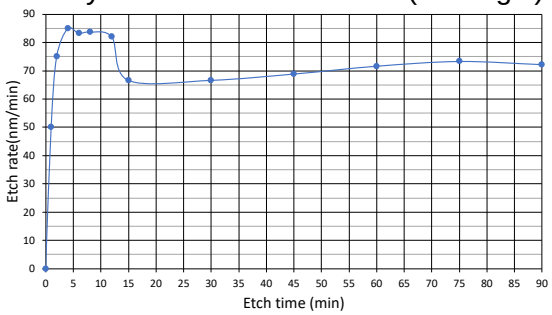

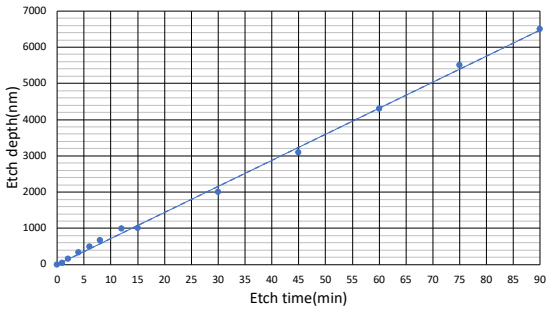

Figure 10: Evolution of a) Etch rate and b) etch depth of a P^- doped diamond layer as a function of time etching at P_{ICP}=500W, P_{Bias}=35W with SiO_2 mask

SEM images in Fig 11 illustrate the diamond films morphologies after etching of 15 min (Fig.11a) and 90 min (Fig.11b). We observe smooth diamond surfaces with no micromasking and trenching at the bottom of trench. An over-etching become visible at the base of the sidewall following a one-hour etching period. The depth of the trenching is assessed at approximately 500 nm using transmission electron microscopy (TEM) analyses conducted on this layer. AFM measurements reported on Fig.12 confirm that the surface roughness is not affected: it is of 0.95 nm after 15 min etching and 0.85 nm after 90 min, due to the good crystal quality free from growth defects.

The depth achieved after 90 min is 6,5 µm corresponding to the required U-gate depth, however the etch profile is not sufficiently anisotropic.

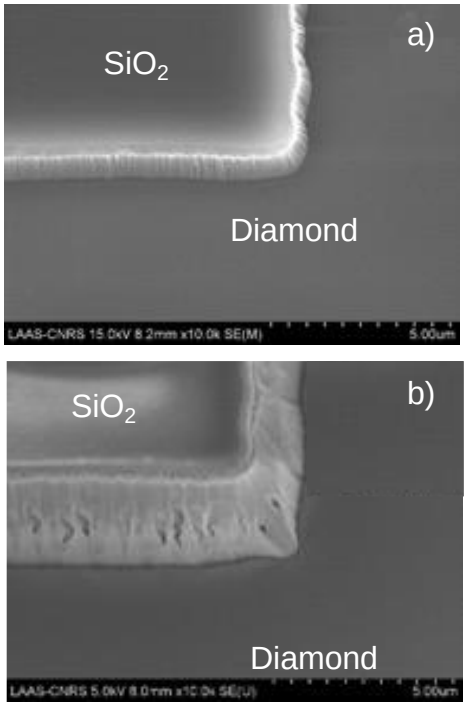

Figure 11: SEM views showing surface of the P- layer a) after 15 min b) after 90 min etching

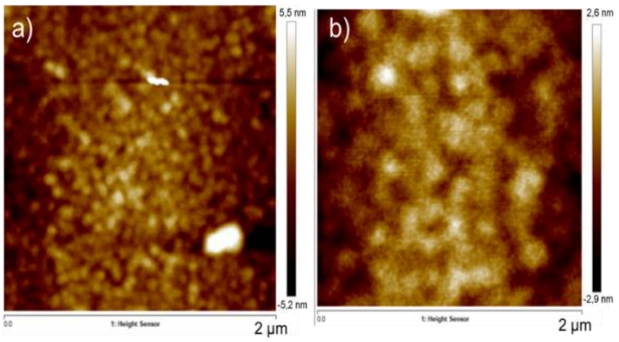

Figure 12: AFM images of the P^- surface roughness a) after 15 min b) after 90 min etching

The etch rate profile is similar whatever the layers type with an increase of the rate in the first minutes of the process followed by a stabilization at a mean value. The etch rate profiles obtained show the existence of two different etch rates, although this has not yet been explained.

The etch rate of the P^- layer and monocrystalline CVD diamond layers are similar, with the absence of micromasking on the etched surface and limited trenching. So, the etching process developed can be used to fabricate the MOSFET gate.

5–Etching process of a $P^+/N/P^-$ layers stack

The cross-sectional view of the vertical P-channel MOSFET with a U-shaped gate, which is the subject of this study, is illustrated in Figure 13. The doping and width of each layer were determined by TCAD simulations, which were conducted with the objective of optimizing the trade-off between breakdown voltage and specific on-resistance (BV/R_{ON}). A portion of the MOS epitaxial structure, constituted by the stacking of P+/N/P- layers on an HPHT 1b substrate, has been specifically grown for the purpose of investigating the U-shaped gate etching process. A P-doped layer was initially epitaxied by MPCVD (microwave plasma chemical vapor deposition) on the HPHT 1b substrate, followed by an N-doped layer and a P^+-doped layer, with a thickness of 8 µm, 2 µm and 3 µm, and doping concentrations of $3x10^{16}$ cm^{-3}, $4.4x10^{17}$ cm^{-3} and $2.3x10^{20}$ cm^{-3} respectively.

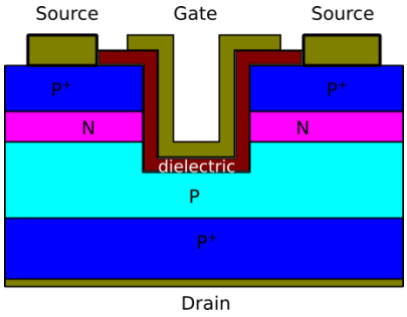

Figure 13: Schematic cross-section of the Up-MOS transistor

We have investigated the influence of the doping concentration and crystallinity of the different doped layers on the resulting etch rate and surface roughness when exposed to the oxygen plasma with a bias power of 35 W.

We have first etched the P^+ layer in order to stop before the P^+/N^- interface. Figure 14.a illustrates the surface state and the etch profile after 30 min etching (2 cycles of 15 min). We can observe anisotropic sidewalls and a defects free surface thanks to the high crystal quality of the P^+ layer. The etch depth measured is 3 µm indicating that we are at the P^+/N^- interface according to the SIMS profiles. The related etch rate is 100 nm/min, instead of 73 nm/min obtained previously for a P^- layer, so the etch rate increases with the boron doping concentration.

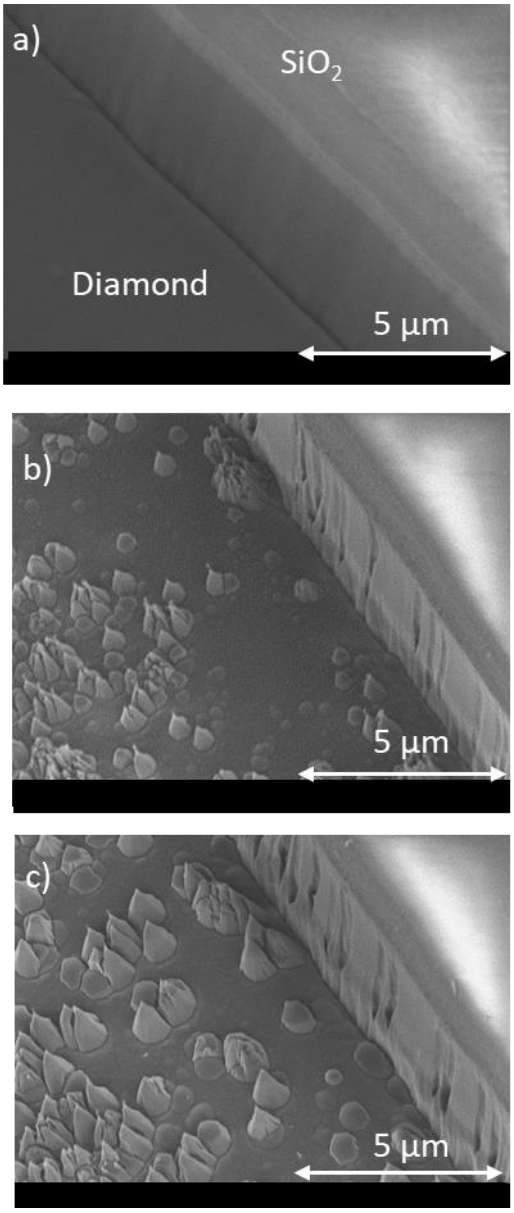

Figure 14: MEB view of a) the 3µm- P+ layer sidewall and resulting etched surface after 30 min of O_2 plasma etching at P_{bias} = 35 W b) $P^+/N^-/P^-$ stack etching after 45 min and c) after 1h

An additional 15 min etching is then performed in order to go through the 2 µm-thick N layer and penetrate the underlying P^- layer. We can observe on Fig 14.b the occurrence of several defects indicating a change in the layers structure and the appearance of trenching at the bottom of the sidewall. By continuing the etching process by steps of 5 min, we observed an increase in the defects size even when reaching the underlying P^- layer (Fig 14.c).

TEM analyses were carried out to determine whether the origin of the defects

appearing on the diamond surface was related to the epitaxy of the P layer or the N layer, and to evaluate the trenching dimensions. A FIB cross-section is made across the sidewall of one of the patterns after 1h etching (Fig 15): in this type of doped layer we observe several surface defects and a trenching depth of 1 µm. The depth value of over-trenching is higher than that observed in the study of the P-layer (4.2), indicating that the depth of trenching may be influenced by the growth conditions. The TEM lamella is shown on Fig 16: we can see a 5.74 µm deep zone with structural defects corresponding to the P^+/N stack.

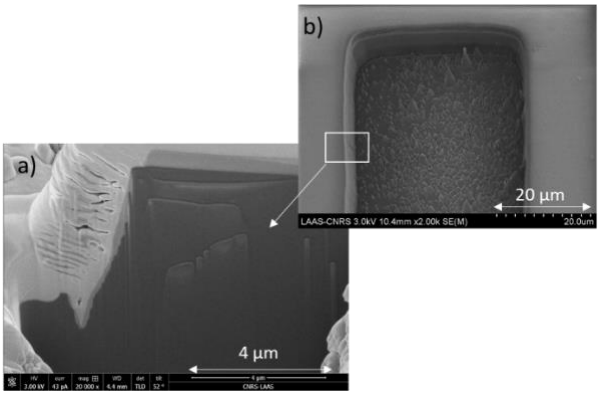

Figure 15: SEM views of a) FIB cross-section across the sidewall for evaluation of trenching b) resulting surface morphology after 1h etch

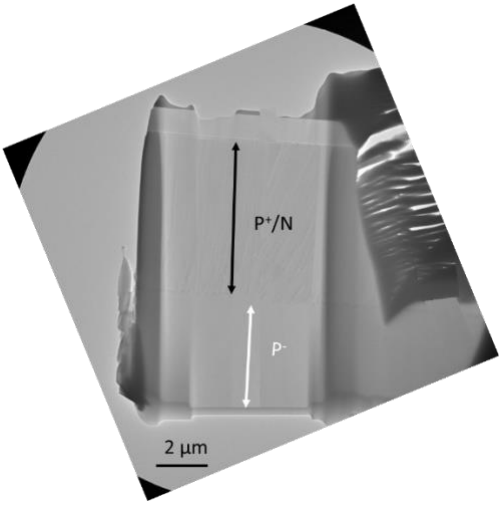

Figure 16: View of the TEM lamella illustrating the P^+/N/P^- stack and the trenching area

TEM analysis in Fig 17.a shows the presence of dislocation defects in the P^+ and N layers, with a higher density in the N layer compared to the P^+ one: not all of these dislocations reach the surface of the P^+ layer. Figure 17.b focuses at the P^+/N interface: the dislocations in the N layer have different orientations and intersect, while those in the P^+ layer are aligned in the same direction.

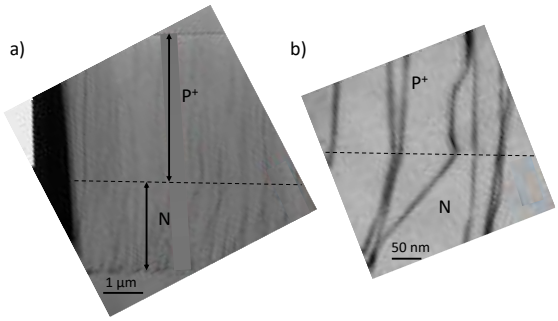

Figure 17: TEM images: a) P^+ and N layers b) lines of defects at the P^+/N interface (dash line)

A line of defects can also be observed at the P^-/N interface with two types of dislocations as reported on the TEM views of Fig 18 i.e linear dislocations and others with loops shape. The presence of a high density of these defects can be explained by the high stresses applied during the deposition of the N layer on the P^- layer.

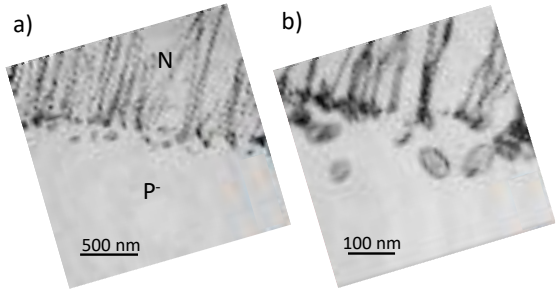

Figure 18: TEM image of defects at the N/P- interface

TEM analysis revealed that the defects appearing on the diamond surface after etching of the N layer were dislocation defects within the crystalline structure of the N layer. At the N/P^- layer interface, other types of dislocations were observed, taking the form of platelets. The SIMS profile of this stack indicates a high concentration of hydrogen at the N/P^- interface. Hydrogen atoms can diffuse into the boron-doped diamond layer and interact to form interstitial platelets.

6-Discussion

The aim being to develop MOSFET devices with a U-shaped gate it is necessary to improve the crystalline quality of epitaxial diamond layers to avoid structural defects revealed by O_2 plasma etching and also to limit the trenching effect, both having a strong influence on the degradation of the electrical characteristics of the power devices.

One way to overcome these issues is to act on the plasma parameters, such temperature and pressure. Increasing the pressure will favor the chemical component of O_2 etching, and also a decrease of P_{bias}, lower than 35 W could limit the impact of the physical component and reduce the trenching. Increasing the temperature will improve the etch rate [28], and we will analyze its impact on trenching.

7- Conclusion

The fabrication of diamond power devices such as TMBS diodes (Trench MOS Barrier Schottky diodes) and vertical P-channel MOSFETs with a U-shaped gate (U-pMOS) requires the development of accurate diamond etching. The aim is to achieve deep etching with an optimal balance between selectivity and low surface roughness avoiding trenching to prevent MOSFET performances degradation, by using both physical sputtering and chemical reactions in the same dry etching process.

We have chosen an oxygen-based etching process that favors the chemical component of RIE etching in order to reduce the effect of over-etching at the bottom of the trench. Aluminum was used first as a hard etching mask with an optimal bias power of 35 W, however it generates significant micromasking during diamond etching. The combination of a pure oxygen plasma and a SiO_2 hard mask with the use of HF buffer after oxide etching resolved significantly micromasking issues.

For single-crystal CVD layers an etch rate of 75 nm\min is obtained with a SiO_2 hard mask and it is similar for P^- doped layers. A higher etch rate of 100 nm/min is achieved when engraving P^+ layers. A lower surface roughness was obtained due to the removal of defects associated with micromasking and the improved epitaxial diamond layer that which contains a reduced ratio of structural defects.

We conclude that the combination of O_2 plasma and SiO_2 hard mask solved the problems of micromasking, and also improved the etch rate to attain the required etch depth.

7- ACKNOWLEDGMENTS AND FUNDING

This work is supported by the French National Research Agency ANR through the MOVeToDIAM project n° ANR-17-CE05-0019-02 and by LAAS-CNRS micro and nanotechnologies platform, member of the French RENATECH network.

The authors would like to thank Éric Imbernon, Adrian Laborde and Pierre-François Calmon for their technical support in the process implementation.

In addition, we would like to express our gratitude to Marie-Amandine Pinault-Thaury from GeMAC and Riadh Issaoui from LSPM for their contribution to the supply of the N and P diamond layers respectively, and the Centre de Microcaractérisation Raimond Castaing for TEM analysis.

8-References

[1] C.J. Wort, R.S. Balmer, Diamond as an electronic material, Mater. Today 11 (1)

[2] R. Makhoul, PhD Thesis, Université de Lyon, 2022.

[3] V.G. Rachenko, T.V. Kononenko, S.M. Pimenov, et al., Diam. Rel.Mater. 2 (1993) 904.

[4] C.J. Chu, C. Pan, J.L. Margrave, R.H. Hauge, Diam. Rel. Mater.4 (1995) 1317.

[5] Q. Sun, M. Alam, J. Mater. Sci. 27 (1992) 5857.

[6] S. Mi, A. Toros, T. Graziosi, and N. Quack, Diamond and Related Materials 92, 248–252 (2019).

[7] T. Nagase, H. Kato, S. A. Pahlovy, and I. Miyamoto, 28(2), 263–267 (2010).

[8] S. Pearton, A. Katz, F. Ren, J.R. Lothian, Electron. Lett. 28 (1992) 63.

[9] B. Stoner, G.J. Tessmer, D.L. Dreifus, Appl. Phys. Lett. 62 (1993) 1803.

[10] A. Vescan, W. Ebert, T.H. Borst, E. Kohn, Diam. Rel. Mater. 5 (1996) 747.

[11] V.G. Ralchenko, K.G. Korotushenko, A.A. Smolin, E.N. Loubnin, Diam. Rel. Mater. 4 (1995) 893.

[12] A. Yoshida, M. Deguchi, M. Kitabatake, et al., Instrum. Methods B 112 (1996) 248.

[13] I. Bello et al. / Thin Solid Films 368 (2000) 222-226

[14] A. Toros, M. Kiss, T. Graziosi, et al, *Diamond & Related Materials* (2020)

[15] D. S. Hwang, T. Saito, and N. Fujimori, Diamond and Related Materials 13(11 –12), 2207 –2210 (2004).

[16] J. Enlund, J. Isberg, M. Karlsson, F. Nikolajeff, J. Olsson, and D. J. Twitchen," Carbon 43(9), 1839 –1842 (2005).

[17] P. Kehayias, A. Jarmola, N. Mosavian, I. Fescenko, F. M. Benito, A. Laraoui, J. Smits, L. Bougas, D. Budker, A. Neumann, S. R. J. Brueck, and V. M. Acosta, Nature Communications 8(1), 188 (2017).

[18] M. Nagai et al., Sci Rep, vol. 8, no 1, p. 1-8, avr.2018.

[19] Adrien Toros.al, Microsystems & Nanoengineering (2018) 4:12

[20] M. Mitchell, D. P. Lake, and P. E. Barclay, APL Photonics 4(1), 016101 (2019).

[21] S.Koné, PhD Thesis, l'Institut National Polytechnique de Toulouse,, 2020.

[22] Fabien Thion, PhD Thesis, INSA de Lyon, 2012.

[23] Gabriel Civrac, PhD Thesis, l'Institut National Polytechnique de Toulouse,, 2009.

[24] Otterbach, R. et al., Diam. Relat. Mater. 10, 511–514(2001).

[25] Chang K. K., ETH Zürich (Doctoral Thesis No. 23962): Zürich, 2016.

[26] Adrien Toros.al, Microsystems & Nanoengineering (2018) 4:12

[27] N. P Johnson, F. Ponce, R. Street, and R. Nemanich, *Phys. Rev. B*, vol. 35, no. 8, pp. 4166–4169, Mar. 1987, doi: 10.1103/PhysRevB.35.4166.

[28] B. J. M. Hausmann, M. Khan, Y. Zhang, T. M. Babinec, K. Martinick, M. McCutcheon, P. R.Hemmer, and M. Lončar, Diamond and Related Materials **19**(5–6), 621–629 (2010).